SUPPORTING INFORMATION

Sustainable co-production of carbon quantum dots and activated carbon from natural rubber latex for the inhibition of pathogenic microorganisms and removal of pharmaceutical residues

Satit Yousatit[a,b], Sakdinun Nuntang[c], Toshiyuki Yokoi[d], Chawalit Ngamcharussrivichai[a,b,*], Napida Hinchiranan [a,b,*]

[a] *Department of Chemical Technology, Faculty of Science, Chulalongkorn University, Pathumwan, Bangkok 10330, Thailand*

[b] *Center of Excellence in Catalysis for Bioenergy and Renewable Chemicals (CBRC), Faculty of Science, Chulalongkorn University, Pathumwan, Bangkok 10330, Thailand*

[c] *Industrial Chemistry Innovation Program, Faculty of Science, Maejo University, Chiang Mai 50290, Thailand*

[d] *Nanospace Catalysis Research Unit, Institute of Integrated Research, Institute of Science Tokyo, 4259 Nagatsuta, Midori-ku, Yokohama 226-8503, Japan*

[*] Corresponding author

E-mail address: Napida.N@chula.ac.th (N. Hinchiranan)

Chawalit.Ng@chula.ac.th (C. Ngamcharussrivichai)

S1. Materials characterization in detail

The structural properties of the carbonaceous materials were analyzed by powder X-ray diffraction (XRD). The XRD pattern was examined using a Bruker D8 ADVANCE diffractometer employing a Cu Kα radiation (λ = 1.5406 Å) at 40 kV and 40 mA with a step size of 0.02° in the 2θ range 5°–75°. The size distributions of CQD nanoparticles were measured by a dynamic light scattering (DLS) technique using a Nanotrac NPA 252 particle size analyzer. Transmission electron microscopy (TEM) was applied to determine the shape and size of obtained CQD using a JEOL JEM-1400 instrument at an accelerating voltage of 80 kV. TEM specimens were prepared by allowing a droplet of the aqueous CQD solution and drying on a carbon grid. The adsorption isotherm and pore size distribution curve of hydrochar and AC were measured at −196 °C using a 3P Micro 300 C1 (3P Instruments, BET-ANAMET) surface area and porosity analyzer. Prior to analysis, the samples were degassed at 150 °C for 2 h. The Brunauer–Emmett–Teller (BET) model and the Horvath and Kawazoe (HK) equation were applied to determine the specific surface area (S_{BET}) and pore size (D_p), respectively. The total pore volume (V_t) was achieved from single point adsorption at relative pressure (P/P_0) of 0.99.

The functional groups of CQD were determined by Fourier transform infrared spectroscopy (FTIR). The FTIR transmittance spectra were recorded at room temperature using a Nicolet iS5 FT-IR spectrometer with attenuated total reflection (ATR) mode at a resolution of 4 cm^{-1} for 64 scans over 400–4000 cm^{-1}. X-ray photoelectron spectroscopy (XPS) was carried out on an AXIS SUPRA photoelectron spectrometer using Al Kα (1486.6 eV) as the X-ray source to analyst the surface functional groups of CQD nanoparticles. The C1s signal was used to calibrate the standard binding energy (BE) at 284.4 eV. The C 1s, O 1s, and N 1s XPS spectra were deconvoluted using OriginPro 8.5 software.

The optical properties of CQD were characterized by UV–Vis absorption and fluorescence spectroscopy. UV–Vis spectra were recorded on a Jasco V-530 spectrophotometer equipped with a deuterium lamp (UV) and a halogen lamp (visible region) at a scan speed of 400 nm min^{-1}. Fluorescence emission spectra were obtained using an Agilent Cary Eclipse spectrophotometer with a xenon lamp as the excitation source. Measurements were carried out at excitation wavelengths ranging from 305 to 395 nm, with a scan rate of 600 nm min^{-1}.

S2. Antimicrobial activity assay in detail

The antimicrobial activity of the CQDs was evaluated against Gram-positive bacteria (*Staphylococcus aureus*, *Micrococcus luteus*, *Bacillus subtilis*), Gram-negative bacteria (*Escherichia coli*, *Klebsiella pneumoniae*), and fungi (*Candida albicans*, *Aspergillus niger*) using disk diffusion and broth dilution methods.

For the disk diffusion assay, bacterial cultures were first adjusted to a turbidity equivalent to a 0.5 McFarland standard (1×10^8 CFU mL^{-1}). Nutrient agar plates were then inoculated with the bacterial suspensions to create a uniform lawn. Sterile disks impregnated with CQDs were placed on the agar surface and the plates were incubated at 37 °C for 24 h in the dark. Following incubation, the zones of inhibition around each disk were measured in millimeters to assess antimicrobial activity.

The broth microdilution method was used to determine minimum inhibitory concentration (MIC) and minimum bactericidal concentration (MBC) of CQD. The test bacteria were cultured in Mueller-Hinton broth (MHB) and incubated at 37 °C for 18 h in a shaking incubator at 150 rpm. Two-fold serial dilutions of CQD were prepared in triplicate using MHB, starting from 120 μg mL^{-1} and diluted on a 96-well plate to a final volume of 200 μL per well.

Each well contained 100 μL of CQD solution and 100 μL of MHB inoculated with bacteria at 1×10^6 CFU mL^{-1}, resulting in final CQD concentrations of 60, 30, 15, 7.5, 3.75, or 1.875 μg mL^{-1}. Plates were incubated at 37 °C under 90% relative humidity for 24 h. Wells containing only MHB and bacteria served as negative controls. MIC was defined as the lowest CQD concentration that inhibited visible bacterial growth relative to the control.

For MBC determination, 10 μL of suspension from wells showing no visible turbidity were spread onto Mueller–Hinton agar (MHA) plates and incubated at 37 °C for 24 h in triplicate. The MBC value was identified as the lowest CQD concentration that resulted in 99.9% bacterial killing.

The time-kill assays and quantitative microbial tests were performed using broth macrodilution method in accordance with the ASTM E2149-10, with minor modifications. Experiments were conducted in 10 mL glass tubes containing 5 mL of CQD solution (140 μg mL^{-1}) and 5 mL of MHB inoculated with bacteria at 1×10^6 CFU mL^{-1}. The tubes were incubated in a shaking incubator at 37 °C and 100 rpm in the dark. Aliquots were collected at 0, 5, 10, 15, 30, 60 min, as well as 24 h. Viable cell counts were determined using a plate count agar method. Briefly, inocula were serially diluted 10-fold in 0.9% sterile saline solution on 96-well microtiter plates, and 10 μL aliquots were spotted onto MHA plates in triplicate. Colony-forming units (CFU) were enumerated after incubation, and the results were expressed as mean CFU mL^{-1} at each time point. Time–kill curves were constructed by plotting the log(CFU mL^{-1}) values versus incubation time. The percentage reduction of viable microbes was calculated according to Eq. (S1)[1]:

$$\%\text{Reduction} = \frac{B - A}{B} \times 100\% \quad \text{(S1)}$$

where A is the number of viable cells after treatment (CFU mL^{-1}), and B is the number of viable cells before treatment (CFU mL^{-1}).

S3. Anti-influenza A virus (H3N2) activity assay in detail

The antiviral activity of CQD against influenza A virus (H3N2) was evaluated using virus inhibition and 50% tissue culture infectious dose ($TCID_{50}$) assays, following ASTM E1053-20 with minor modifications. The Madin–Darby Canine Kidney (MDCK) cells were seeded in 96-well plates with growth medium and incubated at 37 °C for 24 h. The cells were then infected with influenza A virus and incubated for 72 h at 37 °C in a humidified atmosphere containing 5% CO_2. After incubation, the culture supernatant was harvested by centrifugation and stored at −80 °C.

For surface inoculation, virus suspensions were vortexed and spread onto sterile glass Petri dishes to form thin films, which were dried in a controlled chamber. The viral films were subsequently treated with 2.0 mL of CQD dilutions applied via trigger spray and allowed to remain in contact for 5 min. Thereafter, 2.0 mL of neutralizer was added, and the surface was mixed thoroughly. The virus was resuspended by scraping, and the infectious titers were determined by $TCID_{50}$ using the Reed–Muench method.

S4. Adsorption data analysis

S4.1 Quantity adsorbed

The removal efficiency (R, %) and DCF adsorption capacities were calculated according to Eqs. (S2)–(S4)[2]:

$$\textit{Removal efficiency}\ (\%) = \frac{C_0 - C_t}{C_0} x\ 100 \qquad \text{(S2)}$$

$$q_t = \frac{(C_0 - C_t)}{w} V \quad \text{(S3)}$$

$$q_e = \frac{(C_0 - C_e)}{w} V \quad \text{(S4)}$$

where C_0 is initial DCF concentration (mg L^{-1}), C_t is the DCF concentration at time t (mg L^{-1}), and C_e is the equilibrium DCF concentration (mg L^{-1}). q_t and q_e represent the adsorption capacities at time t and at equilibrium, respectively (mg g^{-1}). w is the mass of adsorbent (g), and V is the solution volume (L).

S4.2 Adsorption kinetic models

The adsorption kinetics were investigated by monitoring the concentration of diclofenac (DCF) at different contact times. The experimental data were analyzed using the pseudo-first-order, pseudo-second-order, and Ritchie second-order kinetic models, expressed in Eqs. (S5)–(S7) [3]:

Pseudo-first-order model: $$\ln (q_e - q_t) = \ln q_e - k_1 t \quad \text{(S5)}$$

where q_t and q_e (mg g^{-1}) are the amount of DCF adsorbed at time t and at equilibrium, respectively, and k_1 (min^{-1}) is the pseudo-first-order rate constant determined from the slope of the plot of $\ln (q_e - q_t)$ versus t.

Pseudo-second-order model: $$\frac{t}{q_t} = \frac{1}{k_2 q_e^2} + \frac{t}{q_e} \quad \text{(S6)}$$

where k_2 (g mg^{-1} min^{-1}) is the pseudo-second-order rate constant obtained from the slope and intercept of the plots of t/q_t versus t.

Ritchie second-order model: $$\frac{1}{q_t} = \frac{1}{k_r q_e t} + \frac{1}{q_e} \quad \text{(S7)}$$

where k_r (min^{-1}) is the Ritchie second-order rate constant determined from the plot of $1/q_t$ versus $1/t$.

S4.3 Adsorption isotherms models

The equilibrium adsorption data were analyzed using the Langmuir and Freundlich isotherm models, expressed in Eqs. (S8) and (S9), respectively [4]:

Langmuir isotherm model: $$\frac{1}{q_e} = \frac{1}{q_m} + \frac{1}{k_L q_m C_e} \quad \text{(S8)}$$

where q_e (mg g^{-1}) is the amount adsorbed at equilibrium, q_m (mg g^{-1}) is the maximum adsorption capacity, and k_L (L mg^{-1}) is the Langmuir constant, and C_e (mg L^{-1}) is the equilibrium concentration of DCF.

Freundlich isotherm model: $$\ln q_e = \ln k_F + \frac{1}{n} \ln C_e \quad \text{(S9)}$$

where k_F (mg g^{-1} (L mg^{-1})$^{1/n}$) is the Freundlich constant and n is the Freundlich intensity parameter (dimensionless).

S5. Material characterization and results

Precursor	CQD Type	MIC (μg mL^{-1})	Time	Target microorganisms	Reference
Typha angustifolia	CQD	100	24 h	*P. aeruginosa*	5
Banana peel, grapefruit peel, mangosteen shells, and mango kernels	CQD	1000	24 h	*E. coli*, *S. aureus*, *P. aeruginosa.*	6
Syzygium cumini L.	CQD	500	24 h	*E. coli, K. pneumoniae, S. epidermidis, S.aureus*	7
Vitamin C	CQD	100–300	24–96 h	Bacteria (*S.aureus*, *B. subtilis*, *Bacillus sp.*, *WL-6*, *E. coli*) and fungus (*R. solani, P. grisea*)	8
Guava leaves	Mn-CQD	1160	12 h	*E. coli*	9
Ciprofloxacin and Copper	Cu-CQD	5	24 h	*S. aureus*, *E. coli*	10
Osmanthus leaves	N-doped CQD	~1000	30–60 min	*E. coli*, *S. aureus*	11
m-Aminophenol and tartaric acid	N-doped CQD	250	24 h	*S. aureus*, *E. coli*	12
NR latex and CTAB	N-doped CQD	3.75–15	≤5 min	*S. aureus*, *M. luteus*, *E. coli*, *C. albicans*, *A. niger*, and influenza A virus (H3N2)	This work

Table S1 Comparison of antibacterial activity with previous reports

Table S2 Textural properties of hydrochar and activated carbon samples obtained from different activation methods

Sample	S_{BET}[a] ($m^2\ g^{-1}$)	V_t[b] ($cm^3\ g^{-1}$)	D_p[c] (nm)
Hydrochar	7	0.02	1.96
CAC	994	0.56	1.15
TAC	1167	0.65	1.03

[a] BET surface area

[b] Total pore volume

[c] Pore diameter calculated using the HK micropore analysis

Table S3 Surface elemental composition of hydrochar, CAC, and TAC, analyzed by XPS technique

Atomic orbital	Bond type	Hydrochar		CAC		TAC	
		B.E. (eV)	Conc.[a] (%)	B.E. (eV)	Conc.[a] (%)	B.E. (eV)	Conc.[a] (%)
C1s	C=C, CH_x, C-C	284.3	49.05	284.4	56.35	284.4	70.64
	C−N	285.3	13.55	285.3	11.18	285.4	7.18
	C−O/C−O−C	286.1	9.64	286.1	8.99	286.1	9.81
	C=O	287.6	5.91	287.6	3.40	287.5	4.74
	O=C−O	288.9	2.34	288.8	1.39	288.9	1.61
O1s	O=C	531.5	4.31	531.5	4.28	531.3	1.91
	O−C−O, NO_3	532.6	6.12	532.6	6.50	532.6	1.94
	H−O−C	533.7	2.84	533.7	3.02	533.7	0.84
	O=C−O	535.0	1.32	535.0	0.51	535.1	0.22
N1s	C−N=C	398.9	2.85	398.9	1.50	398.9	0.15
	C−N−C	400.1	1.24	400.1	1.71	400.0	0.25
	$N-C_3$	401.4	0.61	401.4	0.88	401.3	0.62
	N−O	403.1	0.20	403.1	0.28	403.0	0.09
	NO_3	407.5	0.02	-	-	-	-

[a] Atomic concentration.

Table S4 Kinetic parameters of DCF adsorption onto hydrochar, CAC, and TAC

Adsorbent	$q_{e,exp}$ (mg g^{-1})	Pseudo-first order			Pseudo-second order			Ritchie-second order		
		k_1 (min^{-1})	$q_{e,cal}$ (mg g^{-1})	R^2	k_2 (g mg^{-1} min^{-1})	$q_{e,cal}$ (mg g^{-1})	R^2	k_r (L min^{-1})	$q_{e,cal}$ (mg g^{-1})	R^2
Hydrochar	10.88	0.040	3.70	0.221	0.082	11.33	0.982	2.53	11.10	0.063
CAC	116.30	0.042	86.94	0.910	0.001	121.95	0.999	0.13	120.48	0.992
TAC	101.03	0.046	59.2	0.886	0.003	102.04	0.999	0.27	101.01	0.998

Table S5 Isotherm parameters of CFA adsorption onto the CAC adsorbent at 25 °C

Langmuir model			Freundlich model		
k_L (L mg^{-1})	q_m (mg g^{-1})	R^2	n	k_F	R^2
0.582	126.82	0.998	3.10	0.052	0.990

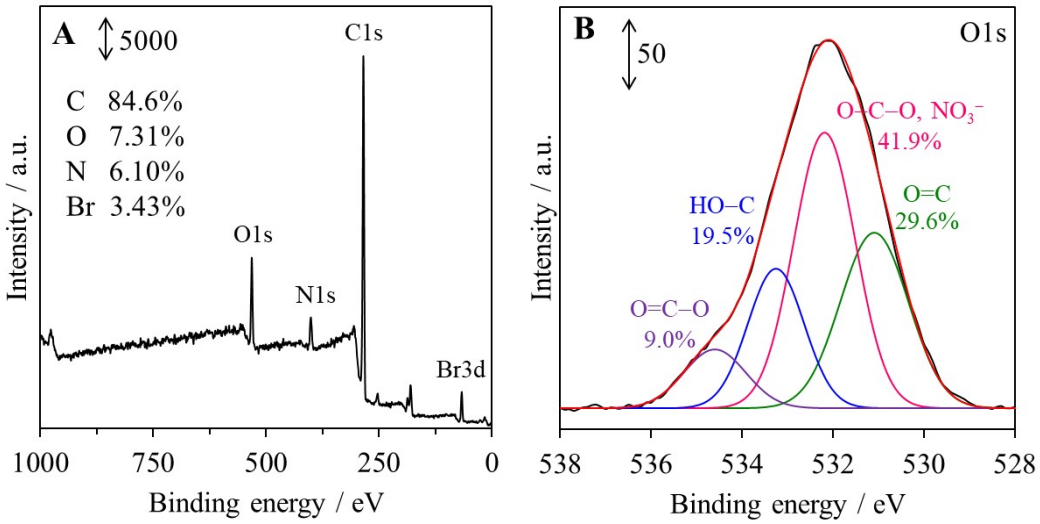

Fig. S1. XPS spectra of CQD: (A) survey scan and (B) high-resolution O1s

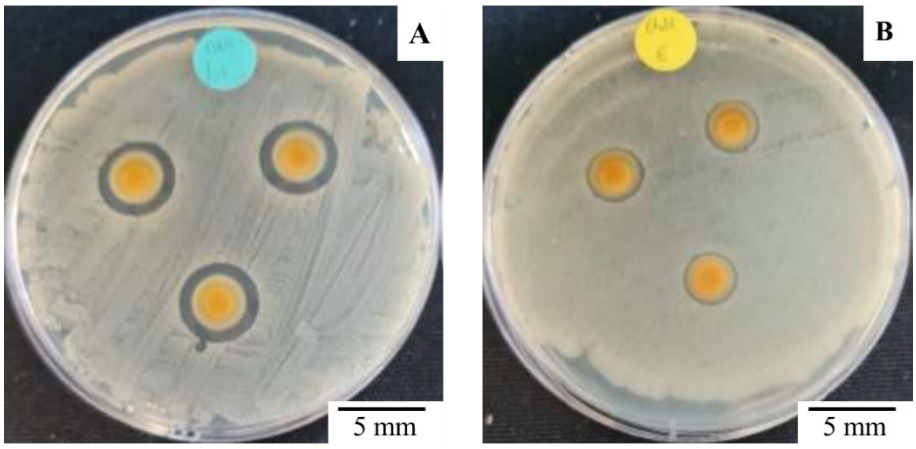

Fig. S2. Antimicrobial activity of CQD against (A) *S. aureus* (Gram-positive) and (B) *E. coli* (Gram-negative) as evaluated by the disk diffusion method. Clear inhibition zones around the disks indicate bacterial growth suppression by CQD.

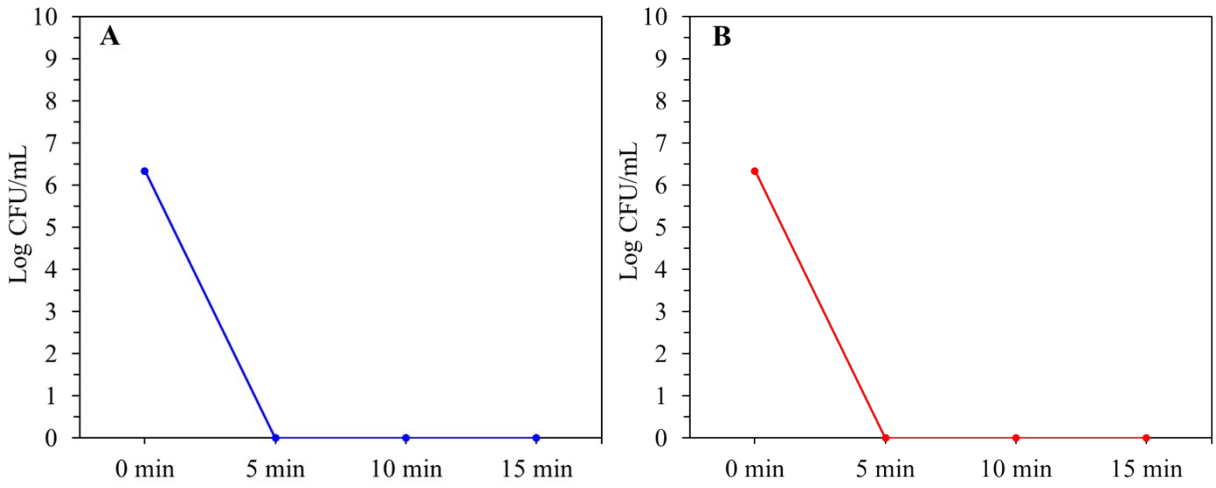

Fig. S3. Time–kill curves for (A) *E. coli* and (B) *S. aureus* following exposure to CQD at their respective minimum bactericidal concentrations (MBC). Bacterial viability was quantified by colony counting at different time intervals, and results are presented as log(CFU mL^{-1}) versus time.

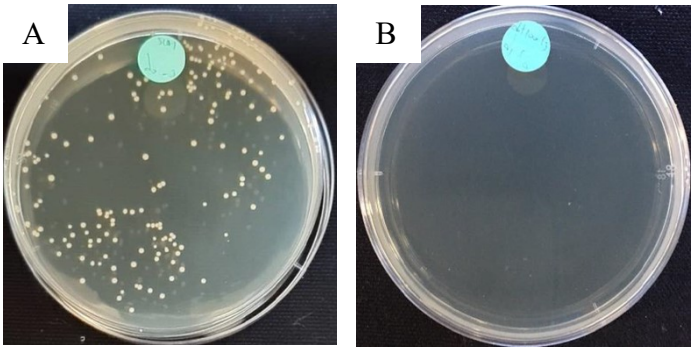

Fig. S4. Regrowth assessment of *S. aureus* after CQD treatment at 0 min (A) and 5 min (B).

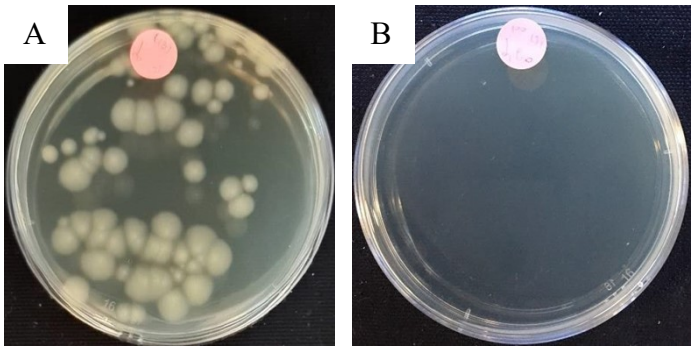

Fig. S5. Regrowth assessment of *E. coli* after CQD treatment at 0 min (A) and 5 min (B).

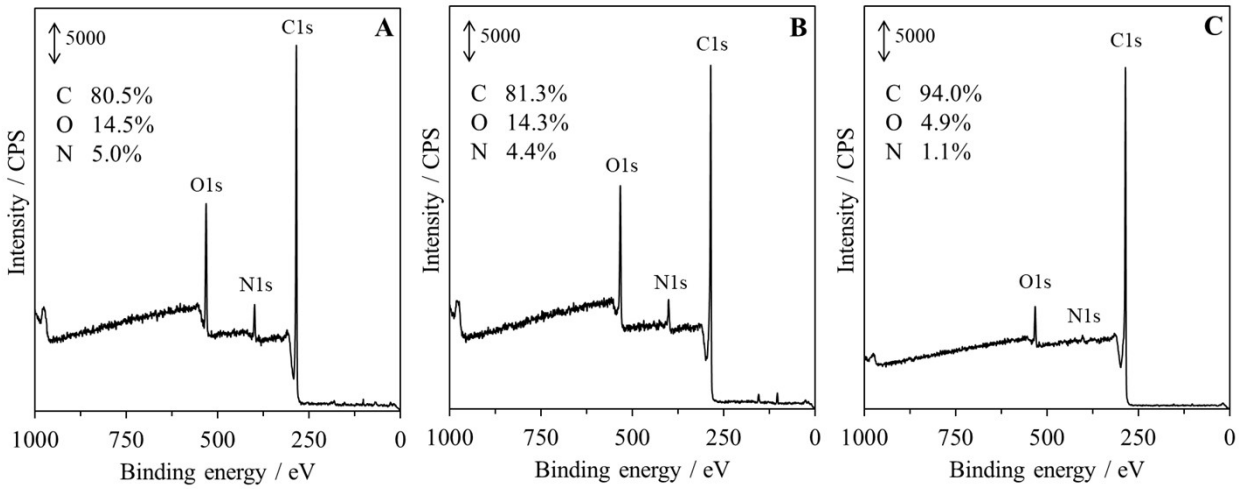

Fig. S6. Survey scan XPS spectra of (A) hydrochar, (B) CAC, and (C) TAC.

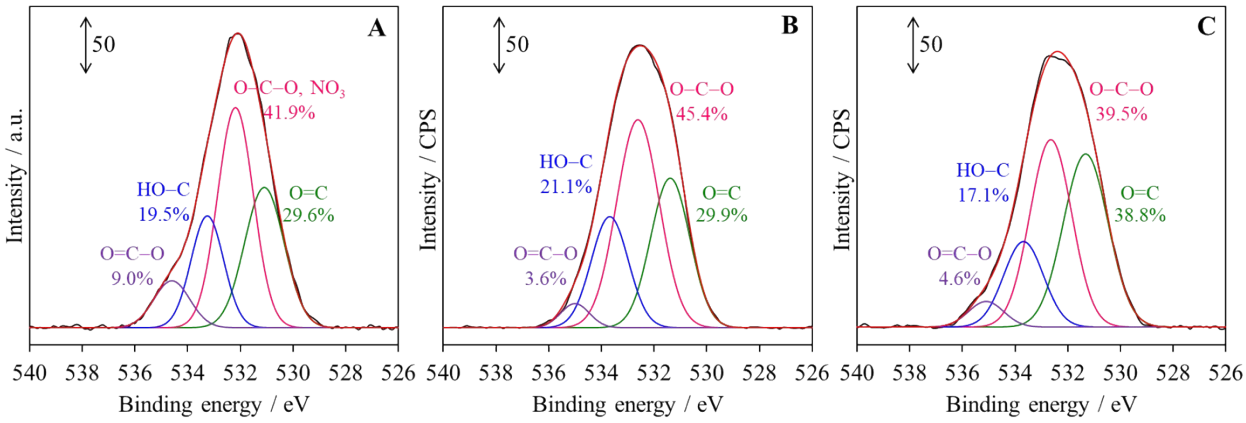

Fig. S7. High-resolution O1s XPS spectra of (A) hydrochar, (B) CAC, and (C) TAC.

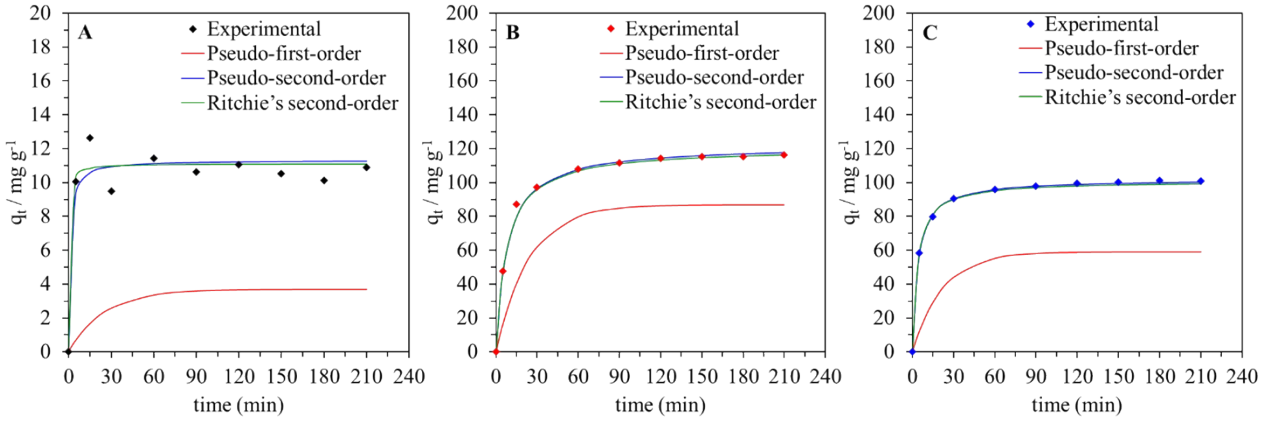

Fig. S8. Adsorption kinetics of DCF onto (A) hydrochar, (B) CAC, and (C) TAC. Experimental data are compared with kinetic model fits (pseudo-first-order, pseudo-second-order, and Ritchie second-order) to evaluate the adsorption mechanism and rate parameters.

References

1. B. I. Elsaba, A. Elsayed, Y. S. Rammah and H. Salaheldin, Correction: Removal of *E. coli* O157:H7 coliform bacteria from sewage wastewater using silver doped borate bioglass, *Sci. Rep.*, 2025, **15**, 34871, https://doi.org/10.1038/s41598-025-22905-3.
2. D. Jagadeesan, H. M. Solayman, C.-J. Hsu, W.-L. Lu, R.-F. Shiu, Y.-F. Lin and J.-J. Jiang, Hierarchical ultra microporous aluminum based metal organic aerogels for water purification: Kinetic, isotherm, and regeneration insights into diclofenac adsorption, *Water Res. X*, 2025, **29**, 100424, https://doi.org/10.1016/j.wroa.2025.100424.
3. K. Ozcan, S. Aydin, S. Emik, A. Öngen and G. W. Kajjumba, *Modelling of adsorption kinetic processes—Errors, theory and application*, in: S. Edebali (Eds.), *Advanced sorption process applications*, IntechOpen, Rijeka, 2018, 80495, https://doi.org/10.5772/intechopen.80495.
4. T. Avcu, O. Üner and Ü. Geçgel, Adsorptive removal of diclofenac sodium from aqueous solution onto sycamore ball activated carbon – isotherms, kinetics, and thermodynamic study, *Surf. Interfaces*, 2021, **24**, 101097, https://doi.org/10.1016/j.surfin.2021.101097.
5. P. Nallasamy, P. Kannan, M. Selvaraj, M. A. Assiri and S. Natarajan, Natural biomass-derived carbon quantum dots: a path to antioxidant, anticancer, antibiofilm, and bacterial bioimaging potential, *Mikrochim Acta*, 2025, **192**, 286, https://doi.org/10.1007/s00604-025-07132-x.
6. Q. Yu, M. Zhang, A. S. Mujumdar and M. Huang, Evaluation of antioxidant, antimicrobial and bacterial labeling capacities of four plant byproduct carbon dots, *Food Biosci.*, 2023, **56**, 103091, https://doi.org/10.1016/j.fbio.2023.103091.

7. R. B. Pricilla, M. Maruthapandi, A. Durairaj, I. Kuritka, J. H. T. Luong and A. Gedanken, Biomass-derived Carbon dots and their coated surface as a potential antimicrobial agent, *Biomass Convers. Biorefin.*, 2023, **14**, 17705–17716, https://doi.org/10.1007/s13399-023-03968-6.

8. H. Li, J. Huang, Y. Song, M. Zhang, H. Wang, F. Lu, H. Huang, Y. Liu, X. Dai, Z. Gu, Z. Yang, R. Zhou and Z. Kang, Degradable carbon dots with broad-spectrum antibacterial activity, *ACS Appl. Mater. Interfaces*, 2018, **10**, 26936–26946, https://doi.org/10.1021/acsami.8b08832.

9. M. Tariq, S. Shivalkar, H. Hasan, A. K. Sahoo and M. P. Sk, Manganese Doping in Biomass Derived Carbon Dots Amplifies White Light-Induced Antibacterial Activity, *ACS Omega*, 2023, **8**, 49460–49466, https://doi.org/10.1021/acsomega.3c08586.

10. H. Miao, P. Wang, Y. Cong, W. Dong and L. Li, Preparation of Ciprofloxacin-Based Carbon Dots with High Antibacterial Activity, *Int. J. Mol. Sci*., 2023, **24**, 6814, https://doi.org/10.3390/ijms24076814.

11. Y. Ma, M. Zhang, H. Wang, B. Wang, H. Huang, Y. Liu and Z. Kang, N-doped carbon dots derived from leaves with low toxicity via damaging cytomembrane for broad-spectrum antibacterial activity, *Materials Today Communications*, 2020, **24**, 101222, https://doi.org/10.1016/j.mtcomm.2020.101222.

12. H. Wang, F. Lu, C. Ma, Y. Ma, M. Zhang, B. Wang, Y. Zhang, Y. Liu, H. Huang and Z. Kang, Carbon dots with positive surface charge from tartaric acid and m-aminophenol for selective killing of Gram-positive bacteria, *J. Mater. Chem. B*, 2021, **9**, 125–130, https://doi.org/10.1039/d0tb02332a.